

SUPPLEMENTAL FIGURES AND LEGENDS

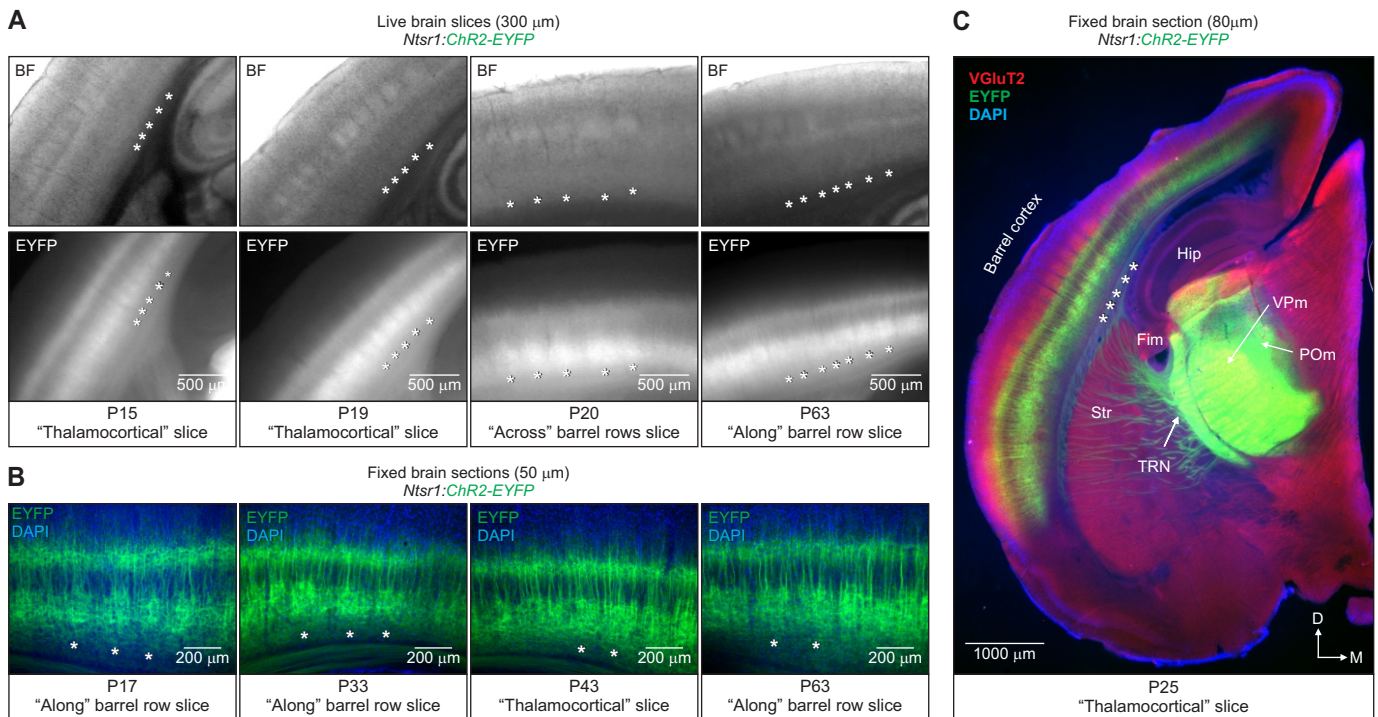


Figure S1. Pattern of cortical EYFP expression in *Ntsr1:ChR2-EYFP* mice of different ages, using various slice planes. Related to Figure 1.

(A) (Top) Examples of bright-field (BF) images taken of live brain slices obtained from various aged *Ntsr1:ChR2-EYFP* mice. Individual slices were 300 μm thick and cut in one of three slice planes: thalamocortical, across barrel rows, or along a barrel row. (Below) Epifluorescence images of the same slices showing that the periodic pattern of EYFP in infragranular layers of cortex (asterisks) was observed in various slice planes of both young (postnatal day 15) and adult mice (postnatal day 63).

(B) Examples of fluorescent images taken of fixed (50 μm) brain sections obtained from mice of different ages. Sections were stained with the nuclear dye DAPI.

(C) Fluorescence image of an entire 80 μm thick section obtained from the same thalamocortical section shown in **Figures 1A and 1B**. The tissue was stained immunohistochemically for VGlut2 and DAPI. Notice that the periodic pattern of EYFP in L6 was restricted to barrel cortex. Hip, hippocampus; Fim, fimbria; Str, striatum, TRN, thalamic reticular nucleus VPm, ventral posterior medial nucleus, POm, posterior medial nucleus.

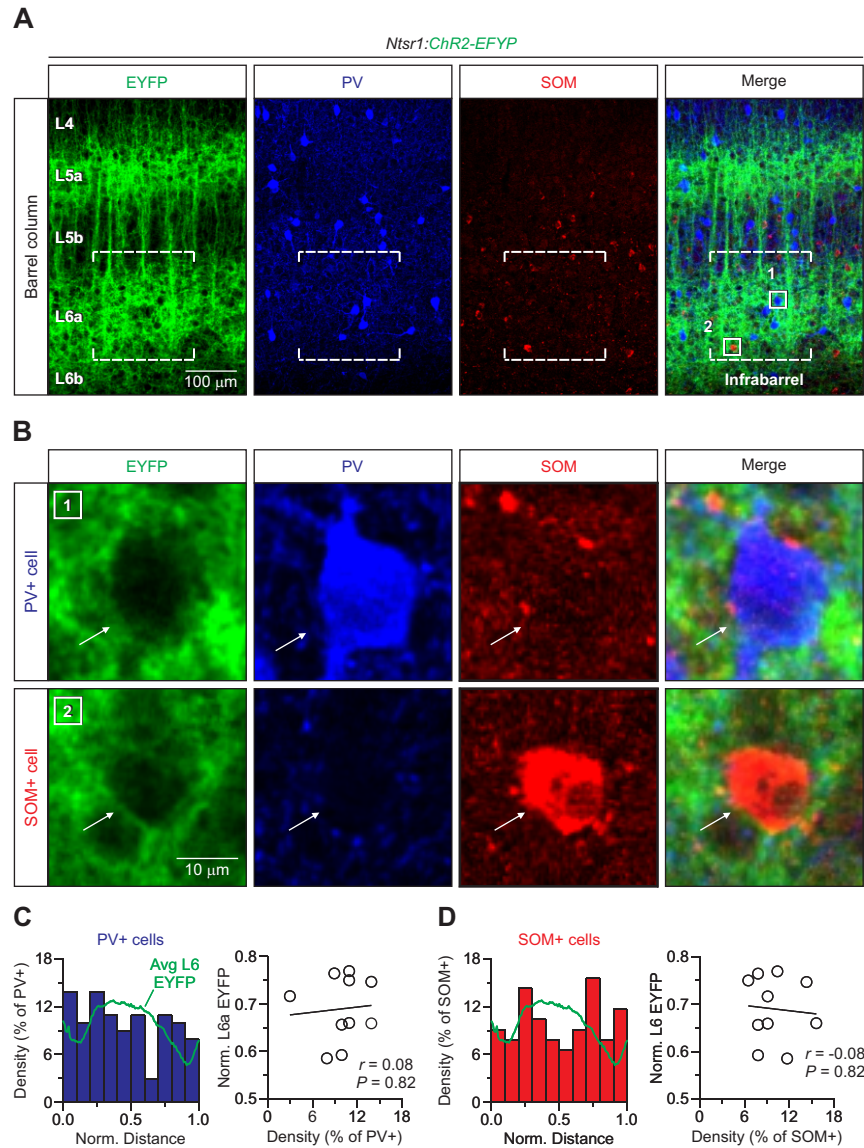


Figure S2. Distribution of parvalbumin- and somatostatin-expressing inhibitory interneurons in L6a of barrel cortex. Related to Figure 3.

(A) Confocal image of a L6a infrabarrel (dashed lines) taken from a 23-day old *Ntsr1:Chr2-EYFP* mouse. Live bright-field images were used to confirm alignment with L4 barrels before fixation. Tissue was stained immunohistochemically for parvalbumin (PV) and somatostatin (SOM).

(B) High magnification image of the boxed areas in (A, far right) showing the two types of labeled cells in L6a.

(C) (Left) A normalized distribution plot of L6a PV-expressing interneurons ($n = 101$ PV-expressing cells, 9 barrel columns, 5 hemispheres, 3 mice). The green trace represents the average fluorescence intensity of L6a EYFP for all columns examined. (Right) Plot showing no correlation between the density of PV-expressing interneurons and L6a EYFP ($r = 0.082$, $p = 0.819$, Pearson's correlation coefficient).

(D) (Left) A normalized distribution plot of L6a SOM-expressing interneurons ($n = 77$ SOM-expressing cells, 9 barrel columns, 5 hemispheres, 3 mice). (Right) Plot showing no correlation between the density of SOM-expressing interneurons and L6a EYFP ($r = -0.080$, $p = 0.824$, Pearson's correlation coefficient).

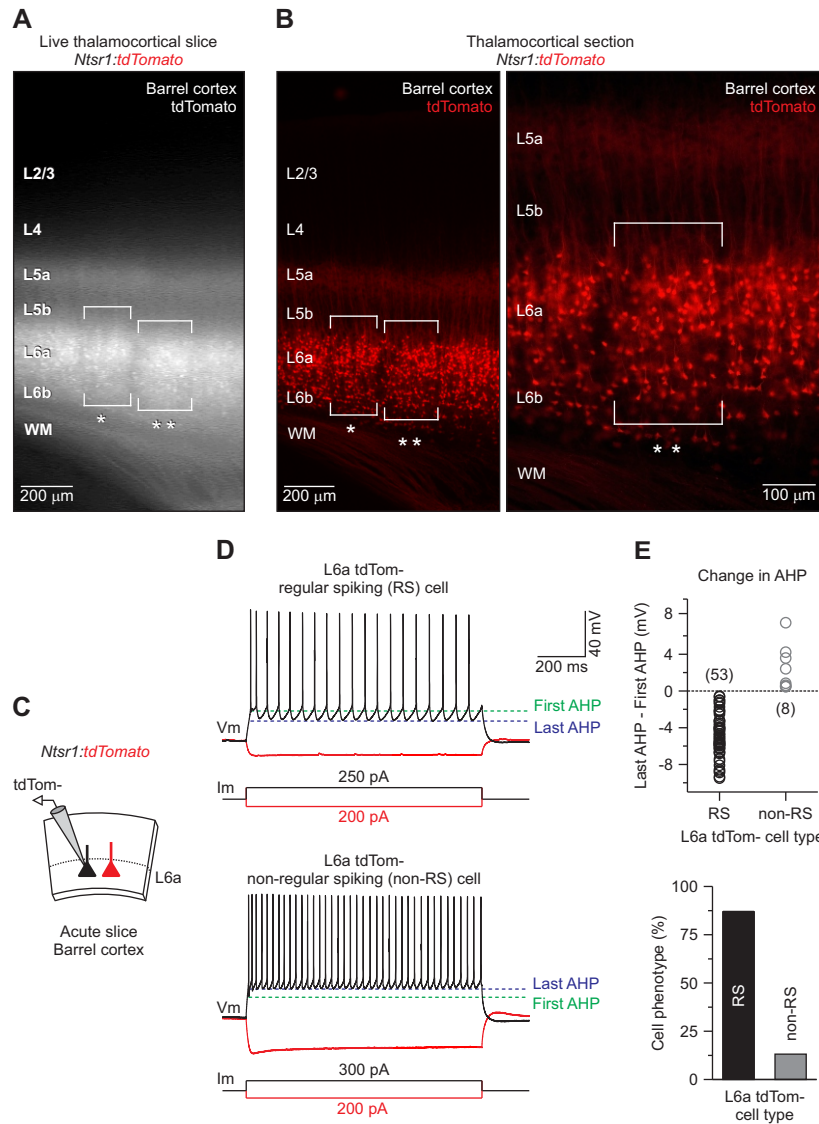


Figure S3. Physiological characterization of tdTomato-negative cells in L6a of barrel cortex from *Ntsr1:tdTomato* mice. Related to Figure 4.

(A) Epifluorescence image of a live 300 μm thick brain slice (along barrel row cut) showing the pattern of tdTomato expression in barrel cortex of a 51-day old *Ntsr1:tdTomato* mouse. Brackets highlight the appearance of two adjacent clusters of L6a CT cells.

(B) Low and high magnification images of a 50 μm thick section taken from the same live slice shown in (A).

(C) Schematic of the slice recording configuration. Whole-cell recordings were made from tdTomato negative cells in L6a barrel cortex of *Ntsr1:tdTomato* mice.

(D) Voltage responses to injected current of two L6a tdTomato-negative neurons. When unambiguous inhibitory interneurons were excluded based on physiological criteria (see **Figure S4**), all remaining cells could be classified as regular-spiking (RS: top) or non-RS neurons (bottom). The two classes of neurons were reliably distinguished by the change in amplitude of afterhyperpolarizations (AHPs) during a 1 second train of action potentials (APs) (Beierlein et al., 2003). For RS neurons, the peak of the AHP after the first AP was always more depolarized than that of the last AHP, whereas for non-RS neurons, the AHP after the first AP was more hyperpolarized. Analysis of AHPs was performed on sweeps in which the firing frequency at the beginning of the train (first interspike interval) was ~50 Hz.

(E) (Top) Summary plot of the change in AHP for all L6a tdTomato negative cells that were not clearly interneurons (Δ AHP: RS cells = -4.83 ± 0.32 mV, $n = 53$ neurons from 27 mice; non-RS = 2.50 ± 0.87 mV, $n = 8$ neurons from 27 mice). (Bottom) Summary histogram showing that ~87% (53 of 61) of the tdTomato negative cells (excluding clearly identified interneurons) in L6a can be identified as having RS physiology.

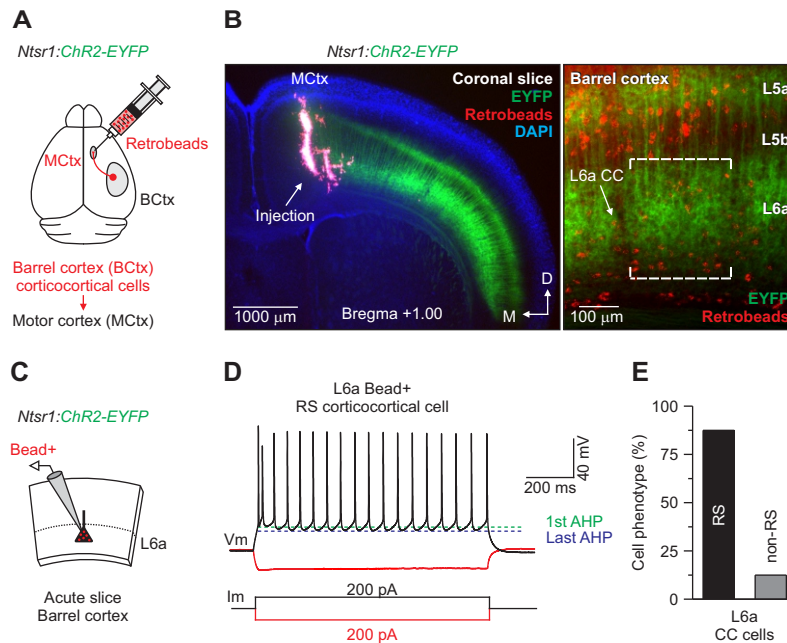


Figure S5. Physiological characterization of L6a corticocortical neurons. Related to Figure 4.

(A) Schematic of the experimental approach. To label L6a corticocortical (CC) cells in somatosensory barrel cortex, we injected fluorescent microspheres (red Retrobeads) in the motor cortex of a *Ntsr1:ChR2-EYFP* mice ($n = 2$ mice). Mice were sacrificed for recordings 4 days after injection.

(B) (Left) Image of an $80 \mu\text{m}$ thick fixed coronal brain section showing the injection site ~ 1 mm anterior and ~ 1 mm lateral of bregma. The tissue was stained with DAPI. (Right) A high-magnification image of barrel cortex, from the same injected mouse, showing retrogradely labeled CC cells (red) in the infragranular layers. Notice the L6a infrabarrel (brackets). (C). Schematic of the slice recording configuration. Whole-cell recordings were made from retrobead-positive cells in L6a of barrel cortex.

(D) Voltage responses of a retrobead-positive, L6a CC cell to injected current.

(E) Summary histogram showing that $\sim 88\%$ (7 of 8) of the retrobead-positive CC cells in L6a could be identified as having RS physiology, based on the negative change in amplitude of their AHPs (ΔAHP : CC cells with RS physiology = -3.4 ± 0.5 mV, $n = 7$ neurons from 2 mice). Based on these results and those presented in **Figure S3**, we conclude that all RS cells in L6a are CC cells. Finally, in 4 of 4 cells tested, L6a CC cells responded to photostimulation with synaptic potential-like latencies (~ 2 ms), indicating they did not express ChR2 (or Cre) ($n = 4$ cells, max light intensity of ~ 30 mW; data not shown).

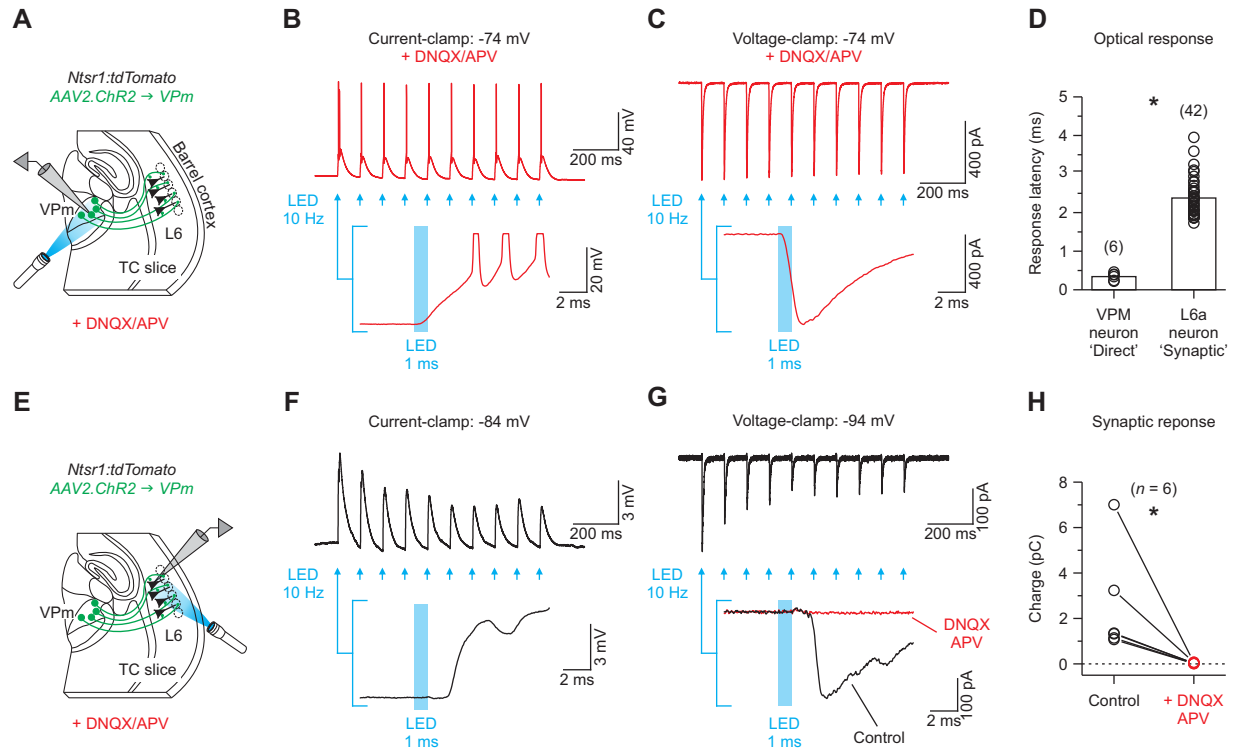


Figure S6. Latencies and glutamate antagonist sensitivity of ChR2-evoked responses. Related to Figure 5.

(A) Schematic of the slice recording configuration. Whole-cell recordings were made from ChR2-expressing VPM neurons to measure responses evoked by wide-field illumination. Selective antagonists of AMPA and NMDA receptors were bath-applied to block fast glutamatergic transmission (DNQX: 20 μ M; APV: 50 μ M).

(B) Voltage responses of a VPM cell to brief flashes of light (1 ms; 10 Hz train; holding potential at -84 mV). The expanded trace shows that the cell depolarized quickly (< 0.6 ms) in response to light. The average light intensity used was 0.83 ± 0.17 mW ($n = 6$ neurons from 1 mouse), which is approximately the average intensity used to evoke the VPM synaptic responses shown in **Figure 5** (0.9 mW).

(C) Current responses of the same VPM cell to brief flashes of light (1 ms; 10 Hz train; voltage-clamp at -74 mV).

(D) Summary plot of the latencies for the direct response in ChR2-expressing VPM neurons and for all optically evoked synaptic response recorded in L6a (Bars represent the mean) (response latency: VPM direct = 0.34 ± 0.04 ms, $n = 6$ neurons from 1 mouse; VPM synaptic = 2.38 ± 0.08 ms, $n = 42$ neurons from 10 mice; $p = 1.63 \times 10^{-7}$, two-tailed Mann-Whitney U -test).

(E) Schematic of the slice recording configuration. Whole-cell recordings were made from L6a neurons to measure synaptic responses evoked by wide-field illumination of ChR2-expressing VPM axons/terminals.

(F) Excitatory postsynaptic potentials (EPSPs) evoked in a L6a CT neuron by brief flashes of light (1 ms; 10 Hz train; light intensity set to 3x EPSP threshold; holding potential at -84 mV; average of 10 trials). The expanded trace shows that the optically evoked EPSPs had delays of ~ 2 ms.

(G) Excitatory postsynaptic currents (EPSCs) evoked in the same L6a neuron (1 ms; 10 Hz train; voltage-clamp at -94 mV; average of 15 trials). Application of DNQX (20 μ M) plus APV (50 μ M) blocked EPSCs (red trace; average of 15 trials).

(H) Summary plot of the effects of DNQX and APV on VPM synaptic responses (EPSC Charge: Control = 2.52 ± 0.04 pC; +DNQX/APV = 0.03 ± 0.02 pC; $n = 6$ neurons from 3 mice, $p = 0.031$, two-tailed paired Wilcoxon signed-rank test).

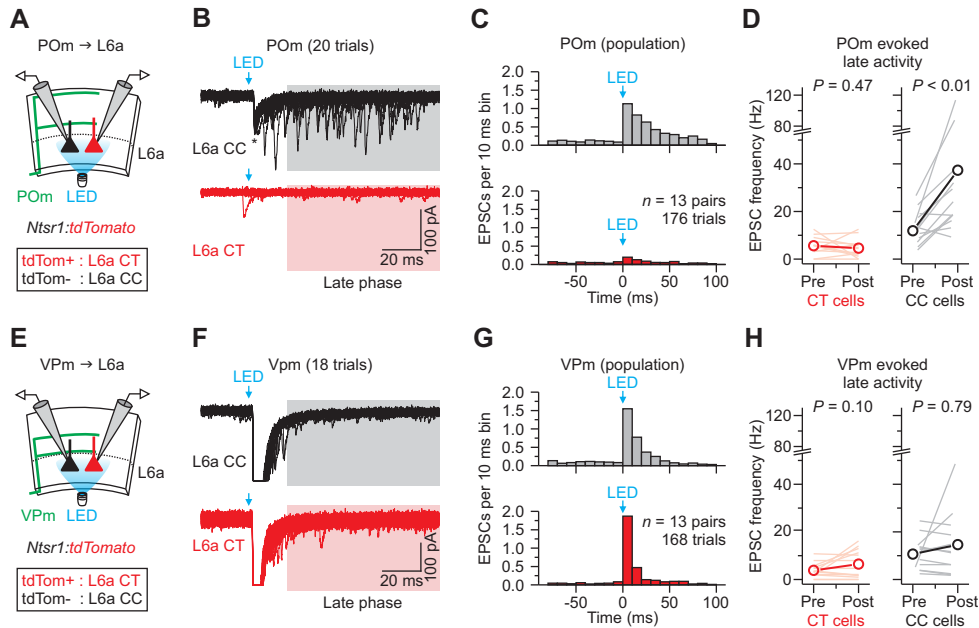


Figure S7. POM-evoked persistent activity in L6a CC cells. Related to Figure 6.

(A) Schematic of the slice recording configuration.

(B) Simultaneously recorded EPSCs for a CT and CC cell pair in response to optical activation of POM axons (1 ms flash of light; intensity set to 3x threshold for evoking an EPSP in the CC cell; cells were held in voltage-clamp at -94 mV). After the fast monosynaptic EPSC (asterisk), there was an increase in the frequency of EPSCs in the CC cell but not the CT cell, occurring 20-100 ms after the pulse (Late phase: shaded regions).

(C) Population peristimulus histogram (10 ms bins) plotting the probability of EPSCs before and after optical activation of POM axons for CT-CC cell pairs ($n = 13$ pairs, 176 trials, from 7 mice; values were calculated by dividing the total number of EPSCs per bin by the total number of trials).

(D) Summary plots showing the EPSC frequency before (80 ms) and after (late phase) photostimulation of POM axons (Circles represent the mean).

(E) Schematic of the slice recording configuration.

(F) Simultaneously recorded EPSCs for a CT and CC cell pair in response to photostimulation of VPm axons (recording conditions were the same as above). Compared with POM, the effects of VPm photostimulation on late activity (shaded regions) were weaker for both CT and CC cells.

(G) Population peristimulus histogram plotting the probability of EPSCs before and after optical activation of VPm axons for CT-CC pairs ($n = 13$ pairs, 168 trials, from 7 mice).

(H) Summary plots showing the EPSC frequency before and after optical activation of VPm axons.

Summary statistics (POM evoked late activity (D): CT Cells: Pre = 5.6 ± 1.0 Hz; Post = 4.6 ± 1.1 Hz; $n = 13$ cells from 7 mice, $p = 0.467$, two-tailed paired t -test; CC Cells; Pre = 11.9 ± 1.9 Hz; Post = 37.3 ± 9.3 Hz; $n = 13$ cells from 7 mice, $p = 0.0017$, two-tailed paired Wilcoxon signed-rank test; VPm evoked late activity (H): CT Cells: Pre = 3.8 ± 0.9 Hz; Post = 6.5 ± 1.6 Hz; $n = 13$ cells from 7 mice, $p = 0.099$, two-tailed paired t -test; CC Cells; Pre = 10.7 ± 1.9 Hz; Post = 14.6 ± 3.9 Hz; $n = 13$ cells from 7 mice, $p = 0.791$, two-tailed paired Wilcoxon signed-rank test). Data are represented as mean \pm SEM.

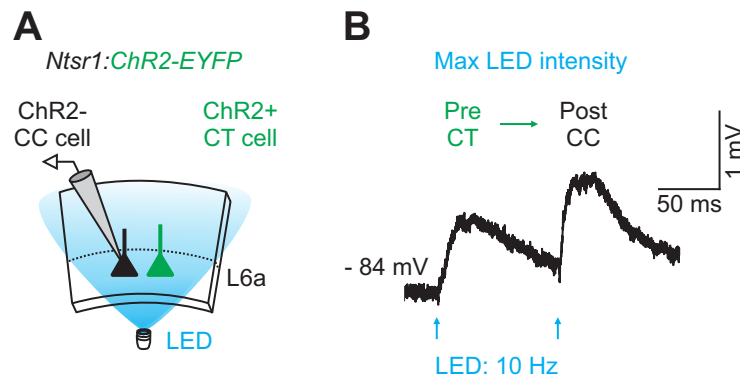


Figure S8. Optogenetic investigation of synaptic connections between L6 CT cells and L6a CC cells. Related to Figure 4.

(A) Schematic of the slice recording configuration. L6a CC cells were identified physiologically by their RS properties. Acute brain slices were prepared from *Ntsr1:ChR2-EYFP* mice.

(B) EPSPs evoked in a L6a CC cell by brief optical activation of L6 CT cells (1 ms light pulses delivered at 10 Hz; trace represents the average of 5 trials). The maximum LED power was used for these experiments (~30 mW at the focal plane). In total, we found that all 10 L6a CC cells recorded ($n = 6$ mice) received synaptic input from L6 CT neurons, with an average EPSP amplitude of 1.8 ± 0.3 mV elicited on the first pulse with max light intensity. All light-evoked responses had EPSP-like latencies (~2 ms), indicating that L6a RS cells did not express ChR2. Although no synaptic connections were found between CT and CC cells with paired recordings (**Figure 4E**), these results imply that CT cells form low probability synapses onto CC cells.

Table S1. Electrophysiological properties of interneurons in layer 6 somatosensory cortex of mice. Related to Figure 4.

	<i>PV-Cre:tdTomato</i>	<i>Som-Cre:tdTomato</i>		<i>5HT3aR-GFP</i>	
		LTS type	FS type	LS type	NLS type
RMP (mV)	-78.9 ± 1.0	-77.0 ± 0.7	-78.5 ± 1.3	-81.4 ± 3.4	-79.8 ± 2.2
R _m (MΩ)	65.9 ± 5.6	200.4 ± 32.4	84.2 ± 16.0	136.8 ± 33.6	373.7 ± 135.4
T _m (ms)	5.7 ± 0.5	17.0 ± 2.0	6.3 ± 1.0	11.8 ± 3.0	14.7 ± 0.5
C _m (pF)	90.8 ± 10.6	89.9 ± 9.7	76.6 ± 3.6	86.2 ± 2.1	51.6 ± 12.2
Rheobase (pA)	560.6 ± 62.4	175.6 ± 20.6	350.0 ± 52.6	171.0 ± 20.9	107.5 ± 30.9
Delay to spike (ms)	105.6 ± 63.8	109.6 ± 10.8	9.6 ± 1.9	773.2 ± 57.6	35.7 ± 6.0
Spike threshold (mV)	-50.0 ± 1.9	-46.7 ± 0.8	-52.2 ± 2.5	-46.3 ± 0.9	-50.2 ± 1.4
Spike amplitude (mV)	69.1 ± 3.5	72.7 ± 2.6	73.5 ± 3.8	60.9 ± 1.8	83.2 ± 5.9
Spike half-width (mV)	0.15 ± 0.00	0.30 ± 0.02	0.18 ± 0.01	0.62 ± 0.04	0.37 ± 0.03
AHP amplitude (mV)	-22.7 ± 1.6	-22.8 ± 1.3	-25.7 ± 1.6	-24.3 ± 0.8	-12.7 ± 1.8
Max rate of rise (mV*ms)	704.6 ± 52.6	498.4 ± 24.8	684.1 ± 47.9	327.1 ± 29.4	638.0 ± 71.5
Max rate of decay (mV*ms)	-614.8 ± 38.5	-293.0 ± 21.6	-545.5 ± 33.5	-87.5 ± 7.0	-214.4 ± 28.6
RMP - threshold (mV)	28.8 ± 2.3	30.3 ± 0.9	26.3 ± 2.1	35.1 ± 3.7	29.5 ± 2.9
Spike frequency adaptation ratio (Last/1st)	0.65 ± 0.05	0.44 ± 0.03	0.76 ± 0.06	0.96 ± 0.07	0.31 ± 0.11
Voltage sag amplitude (mV)	-1.0 ± 0.1	-2.7 ± 0.3	-1.2 ± 0.4	-1.2 ± 0.2	-4.4 ± 1.6
	(n = 8 cells, 2 mice)	(n = 8 cells, 3 mice)	(n = 4 cells, 3 mice)	(n = 5 cells, 3 mice)	(n = 4 cells, 3 mice)

* See Experimental Procedures for an explanation of how the electrophysiological parameters were defined/measured. Data are represented as mean ± SEM.

* All membrane potentials were corrected for a 14 mV liquid junction potential

Table S2. Electrophysiological properties of corticothalamic (CT) and corticocortical (CC) neurons in layer 6a somatosensory cortex of mice. Related to Figure 4.

	<i>Ntsr1-Cre:tdTomato</i>				<i>P</i>	Test
	L6a CT Cell		L6a CC Cell			
	(tdTomato positive)		(tdTomato negative + RS physiology)			
	Mean \pm s.e.m.	<i>n</i> cells / <i>n</i> mice	Mean \pm s.e.m.	<i>n</i> cells / <i>n</i> mice		
RMP (mV)	-83.7 \pm 0.3	87 / 32	-84.2 \pm 0.4	52 / 27	0.51391	Mann-Whitney <i>U</i> -test
R _m (M Ω)	182.2 \pm 12.0	52 / 24	147.1 \pm 10.7	32 / 20	0.03480	Mann-Whitney <i>U</i> -test
τ_m (ms)	15.2 \pm 0.7	52 / 24	19.5 \pm 1.0	32 / 20	5.22 \times 10 ⁻⁵	Mann-Whitney <i>U</i> -test
C _m (pF)	87.9 \pm 2.1	52 / 24	144.6 \pm 8.0	32 / 20	6.44 \times 10 ⁻¹¹	Mann-Whitney <i>U</i> -test
Rheobase (pA)	190.0 \pm 12.2	31 / 16	112.4 \pm 8.2	21 / 12	1.64 \times 10 ⁻⁵	<i>t</i> -test
Delay to spike (ms)	468.0 \pm 60.0	31 / 16	220.6 \pm 38.7	21 / 12	0.05187	Mann-Whitney <i>U</i> -test
Spike threshold (mV)	-45.3 \pm 0.5	31 / 16	-50.5 \pm 0.8	21 / 12	2.18 \times 10 ⁻⁷	<i>t</i> -test
Spike amplitude (mV)	72.6 \pm 1.4	31 / 16	82.6 \pm 1.3	21 / 12	7.88 \times 10 ⁻⁷	<i>t</i> -test
Spike half-width (mV)	0.58 \pm 0.01	31 / 16	0.67 \pm 0.02	21 / 12	3.47 \times 10 ⁻⁵	<i>t</i> -test
AHP amplitude (mV)	-18.5 \pm 0.4	31 / 16	-19.8 \pm 0.6	21 / 12	0.06952	<i>t</i> -test
Max rate of rise (mV*ms)	429.1 \pm 19.5	31 / 16	526.2 \pm 23.0	21 / 12	0.00238	<i>t</i> -test
Max rate of decay (mV*ms)	-126.8 \pm 2.7	31 / 16	-108.5 \pm 4.5	21 / 12	5.03 \times 10 ⁻⁴	<i>t</i> -test
RMP - threshold (mV)	38.7 \pm 0.7	31 / 16	33.5 \pm 0.9	21 / 12	5.65 \times 10 ⁻⁵	<i>t</i> -test
Spike frequency adaptation ratio (2nd/1st)	0.74 \pm 0.01	76 / 32	0.60 \pm 0.02	49 / 27	5.36 \times 10 ⁻¹¹	<i>t</i> -test
Spike frequency adaptation ratio (Last/1st)	0.52 \pm 0.01	73 / 30	0.44 \pm 0.02	46 / 25	3.05 \times 10 ⁻⁴	Mann-Whitney <i>U</i> -test
AHP change (mV)	0.6 \pm 0.3	75 / 32	-4.8 \pm 0.3	53 / 27	8.69 \times 10 ⁻²²	<i>t</i> -test
Voltage sag amplitude (mV)	-4.3 \pm 0.2	76 / 32	-2.2 \pm 0.2	49 / 27	9.93 \times 10 ⁻¹⁴	Mann-Whitney <i>U</i> -test

* See Experimental Procedures for an explanation of how the electrophysiological parameters were defined/measured. Data are represented as mean \pm SEM.

* All membrane potentials were corrected for a 14 mV liquid junction potential

* All statistical tests were two-tailed

SUPPLEMENTAL EXPERIMENTAL PROCEDURES

Retrograde Labeling. Red fluorescent latex microspheres (RetroBeads, Lumafluor) were injected at full concentration in *Ntsr1:Ai32* mice (n = 2 mice; postnatal age = 28 and 29 days). The same surgical procedures were used as described above (see virus injections). Retrobeads were injected in 4 locations surrounding the vibrissa region of motor cortex, to label L6 CC neurons (coordinates from bregma for motor cortex were 0.8 - 1.0 mm lateral, 0.95 - 1.05 mm anterior, and 0.4 and 0.8 mm depth) (Ferezou et al., 2007; Hooks et al., 2013; Mao et al., 2011). The total volume per mouse was 0.3 – 0.4 μ l. Mice were sacrificed for slice physiology 4 days after bead injection.

Electrophysiological Data Analysis. Excitatory connections. To test for the presence of excitatory connections between L6 CT and CC (RS) cells, depolarizing current pulses (1 s duration; 50 pA steps) were applied to evoke a train of action potentials (APs) in the presynaptic cells. Excitatory connections were determined *post hoc* by examining spike-triggered averages of postsynaptic responses to the first, third, and all APs in the trains. In 2 of the 4 excitatory connections found, short (2 - 3 ms) current pulses (1.5 – 2.0 nA) were applied to evoke an AP in the presynaptic neuron (4 - 5 pulses at 10 – 20 Hz). The amplitude of an evoked EPSP was measured relative to a baseline before the stimulus (0.2 - 10 ms). Both cells were held at a holding potential of -84 mV when testing for the presence of excitatory connections.

Intrinsic properties. Resting membrane potentials (RMP, in mV) were measured within 1 min of break-in, with no current applied. Only cells with stable membrane potentials were included. Input resistances (R_{in} , in $M\Omega$) were determined using Ohms Law by measuring the voltage response, from rest, in response to small negative current injections (5 - 20 pA; 500 ms duration; 7-99 sweeps; \sim 1.5 mV mean response). Membrane time constants (τ_m , in ms) were measured from the average voltage response (see input resistance above) by fitting a single exponential to the initial falling phase of the response (100 ms; omitting the first 1 ms). For a few cells with particularly short time constants, a shorter window was used to obtain a better fit. Input capacitance (C_{in} , in pF) was calculated as τ_m / R_{in} . Rheobase currents (in pA) were defined as the minimal positive current injection needed to evoke an AP from a holding potential of -84 mV (1000 ms pulse duration; 5 pA steps). AP latencies (in ms) were determined by measuring the time from the start of the rheobase current pulse to the peak of the first AP. AP thresholds (in mV) were determined from the first AP evoked by the rheobase current and defined by the membrane potential at which the dV/dt of the AP exceeded 10 mV/ms. AP amplitudes (in mV) were determined for the first AP evoked by the rheobase current and measured as the difference between the threshold and the peak of the AP. AP half-widths (in ms) were determined for the first AP evoked by the rheobase current and measured at the half height between threshold and the peak of the AP. The max rate of rise (in mV/ms) was defined as the maximal dV/dt during the upswing of the first AP evoked by the rheobase current. The max rate of decay (in mV/ms) was defined as the maximal negative dV/dt during the downswing of the first AP evoked by the rheobase current. Afterhyperpolarizations (AHPs; in mV) were measured as the difference between the threshold and the peak of the AHP. Spike frequency adaptation was determined by calculating the adaptation ratio, defined as the firing frequency at the second or last interspike interval divided by the firing frequency at the first interspike interval. For CT and CC cells, analysis was performed on a 1 s depolarizing current step that generated sustained firing in which the initial firing rate was near 50 Hz. For interneurons, analysis was performed on the smallest current step that generated sustained firing. The change in amplitude of AHPs (in mV) was defined as the amplitude differences between the first and last AHP elicited by a 1 s depolarizing current step. Analysis was performed on sweeps in which the firing frequency at the beginning of the train (first interspike interval) was near 50 Hz. Peak sag amplitudes (in mV) were measured in response to a 1 s negative current step (-200 pA for CT and CC cells; -100 pA for interneurons) and calculated relative to the steady-state voltage at the end of the step (average of last 200 ms). Analysis of electrophysiological data was performed using Molecular Devices Clampfit 10, AxoGraph X, and Microsoft Excel.

Histology. Immunohistochemistry. All tissue for immunohistochemistry was prepared from acute brain slices (see above, *in vitro* slice preparation), except for tissue cut in the tangential plane, which was prepared via transcardial perfusion. Acute brain slices containing L6 infrabarrels were transferred to a 4% paraformaldehyde in 0.1 M phosphate buffer solution overnight at 4°C (18 – 24 hours). The next day, slices were changed to a 30% sucrose in 0.1 M phosphate buffer solution until re-sectioned (4°C; 2 – 3 days). Tissue was re-sectioned between 40 and 80 μ m (typically 80 μ m) using a freezing microtome and immunostained as described previously (Neske et al., 2015). We found that infrabarrels were much more discernible in 80 μ m thick sections. Briefly, sections were washed twice in 0.1 M phosphate buffer followed by 3 washes in 0.1 M phosphate buffer with 0.15 M NaCl, pH 7.4 (PBS, 5 min per wash). After washing, sections were incubated for 1 hour at room temperature in a blocking solution containing 0.1% Tween, 0.25% Triton X-100, 10% normal goat serum in PBS, then incubated with primary antibody for 3-4 days with

rotation at 4°C. Following primary incubation, sections were washed 5 times in PBS (5 min per wash). After washing, tissue was pre-blocked for 45 min in blocking solution (same as above), then incubated with secondary antibody for 2 hours at room temperature, washed 3 times in PBS (10 min each), followed by 2 rinses in PB (5 min each). All sections were mounted and coverslipped using Vectashield or Vectashield with DAPI (Vector laboratories H-1000 or H-1200). Primary antibodies used were mouse monoclonal anti-NeuN (1:1000; Millipore MAB377), guinea pig polyclonal anti-VGluT2 (1:12000; Millipore AB2251), mouse monoclonal anti-parvalbumin (1:2000; Swant clone 235), and rabbit polyclonal anti-somatostatin-14 (1:1000; Bachem T4103). VGluT2 (vesicular glutamate transporter 2) labels the presynaptic terminals of thalamocortical axons (Fremeau et al., 2001), whereas NeuN is a neuron-specific marker (Mullen et al., 1992). Secondary antibodies used were goat anti-guinea pig IgG (H+L) Alexa Fluor 568 (1:500; Molecular Probes A11075), goat anti-guinea pig IgG (H+L) Alexa Fluor 488 (1:500; Molecular Probes A11073), goat anti-mouse IgG (H+L) Alexa Fluor 633 (1:500; Molecular Probes A21052), and goat anti-rabbit IgG (H+L) Alexa Fluor 568 (1:500; Molecular Probes A11036).

Tangential sections. Mice were anesthetized with Beuthanasia (360 mg/kg) and transcardially perfused with PBS containing heparin (3 U/ml), followed by 4% paraformaldehyde in 0.1 M phosphate buffer. The brain was removed, and the cortex was dissected from the underlying structures. The cerebral hemispheres were then flattened between two glass slides that were held loosely with rubber bands and placed in 4% paraformaldehyde in 0.1 M phosphate buffer solution for 2 hours at 4°C. After fixation, the glass slides were removed and the tissue was then incubated in 0.1 M phosphate buffer solution overnight at 4°C (18 – 24 hours). The following day, the cerebral hemispheres were changed to a 30% sucrose in 0.1 M phosphate buffer solution until sectioned at 80 µm (4°C; 2 – 3 days).

Cytochrome oxidase staining. Brain sections cut tangential to the pial surface (80 µm) were washed 3 times in 0.1 M phosphate buffer (5 min per wash). After washing, sections were incubated in the dark for 12 - 18 hours with rotation at room temperature in a solution containing 4% sucrose, 0.035% cytochrome oxidase, 0.02% catalase, 0.05% DAB (Sigma) in PB. Following incubation, sections were washed twice with 0.1 M phosphate buffer, mounted on subbed slides, dehydrated with ethyl alcohol solutions (70 – 100%) and xylene, and then coverslipped using Vectashield.

For histology, the age range of mice used was from postnatal day 15 to 64 (**Figures 1B and 1C**: n = 6 total mice, 4 mice at p25 and 2 mice at p47; **Figures 1D and 1E**: n = 2 total mice at p26; **Figure 2B**: n = 2 total mice at p34; **Figure 2C**: n = 2 total mice at p54; **Figure 3**: n = 3 total mice at p25; **Figure S1**: n > 27 mice ranging from p15 to p64; **Figure S2**: n = 3 total mice at p23; **Figure S5**: n = 2 total mice at p28 and p29).

Microscopy. Images of acute brain slices were taken using bright-field illumination and fluorescence microscopy with a Nikon Eclipse E600FN microscope equipped with a high-resolution camera (Andor Zyla 5.5 CMOS camera, Solis software; Objective: Nikon 4x / 0.1 NA). Some live slice images were taken using the Zeiss system described above (Zeiss Plan Neurofluor 2.5x / 0.075 NA; see *In Vitro* Recordings and Data Acquisition). During imaging, live slices were kept in a submersion recording chamber and continually bathed with oxygenated ACSF. Images of fixed tissue were taken using a SPOT Camera (Diagnostic Instruments SPOT RT220-3 camera, SPOT software) mounted to a Nikon Eclipse E600 microscope equipped with the appropriate filter sets (Nikon Plan APO 4x / 0.2 NA or Nikon Plan APO 10x / 0.45 NA;). Confocal image stacks of immunostained tissue were taken on a Zeiss LSM 510 Meta confocal laser scanning microscope equipped with updated Zen software (Objectives: Zeiss C Aplanachromat 40x Water / 1.2 NA, Zeiss Plan Aplanachromat 20x / 0.8 NA, or Zeiss Plan Aplanachromat 5x / 0.16 NA; laser excitation wavelengths: 405 nm, 488 nm, 561 nm, and 633 nm). Brightness and contrast were adjusted offline using Fiji software (Schindelin et al., 2012).

Cell Counting. Image processing and cell counts were performed using Fiji, an open source image processing package (Schindelin et al., 2012). To assure cell counts were performed on an intact barrel column, we limited our analysis to the middle of 3 adjoining infrabarrels that were all aligned with L4 barrels, as defined by the L4 VGluT2 expression or live images. High-resolution confocal image stacks of a barrel column were reconstructed using the Pairwise Stitching plugin with subpixel accuracy (Preibisch et al., 2009). Overlapping areas were merged using a linear blend or average function. All images were visually inspected for accuracy and re-processed with an increased number of peaks if the stitching was not correct. The upper and lower borders of L6a were determined by measuring the EYFP fluorescence as a function of distance across cortical layers (that is, from pia to white matter) for a ~50 µm region through the two neighboring columns. The L5b/L6a border was defined as ~0.8 of peak normalized fluorescence, whereas the L6a/b border was defined as 0.5 of peak normalized fluorescence. Lines were then drawn between these marks, creating the upper and lower borders of L6a. Cell counts were performed between these lines using the Fiji Cell Counter plugin. Only one section per hemisphere was used for counts to avoid analyzing the same barrel column

in adjacent sections. Control cell counts confirmed that 97.5% of L6 CT cells (initially identified via membrane EYFP) were labeled with NeuN across the depths used for counts (n = 512 of 525 L6 CT cells, 8 barrel columns, 4 hemispheres, 3 mice). NeuN-positive cells that could not be definitively assigned based on EYFP fluorescence were left uncategorized and excluded from the total number of cells. To quantify the distribution of cells across multiple barrel columns, and to avoid confounding factors such as differences in column size, the final horizontal position (across L6a) for each cell was normalized to the lateral borders of the neighboring septa, defined by either the L4 VGluT2 or L6a EYFP fluorescence.

SUPPLEMENTAL REFERENCES

- Beierlein, M., Gibson, J.R., and Connors, B.W. (2003). Two dynamically distinct inhibitory networks in layer 4 of the neocortex. *J Neurophysiol* 90, 2987-3000.
- Cruikshank, S.J., Ahmed, O.J., Stevens, T.R., Patrick, S.L., Gonzalez, A.N., Elmaleh, M., and Connors, B.W. (2012). Thalamic control of layer 1 circuits in prefrontal cortex. *J Neurosci* 32, 17813-17823.
- Freneau, R.T., Jr., Troyer, M.D., Pahner, I., Nygaard, G.O., Tran, C.H., Reimer, R.J., Bellocchio, E.E., Fortin, D., Storm-Mathisen, J., and Edwards, R.H. (2001). The expression of vesicular glutamate transporters defines two classes of excitatory synapse. *Neuron* 31, 247-260.
- Hu, H., Cavendish, J.Z., and Agmon, A. (2013). Not all that glitters is gold: off-target recombination in the somatostatin-IRES-Cre mouse line labels a subset of fast-spiking interneurons. *Frontiers in neural circuits* 7, 195.
- Mullen, R.J., Buck, C.R., and Smith, A.M. (1992). NeuN, a neuronal specific nuclear protein in vertebrates. *Development* 116, 201-211.
- Neske, G.T., Patrick, S.L., and Connors, B.W. (2015). Contributions of diverse excitatory and inhibitory neurons to recurrent network activity in cerebral cortex. *J Neurosci* 35, 1089-1105.
- Preibisch, S., Saalfeld, S., and Tomancak, P. (2009). Globally optimal stitching of tiled 3D microscopic image acquisitions. *Bioinformatics* 25, 1463-1465.
- Rudy, B., Fishell, G., Lee, S., and Hjerling-Leffler, J. (2011). Three groups of interneurons account for nearly 100% of neocortical GABAergic neurons. *Developmental neurobiology* 71, 45-61.
- Schindelin, J., Arganda-Carreras, I., Frise, E., Kaynig, V., Longair, M., Pietzsch, T., Preibisch, S., Rueden, C., Saalfeld, S., Schmid, B., *et al.* (2012). Fiji: an open-source platform for biological-image analysis. *Nat Methods* 9, 676-682.